BAYESIAN ESTIMATION OF INTERNAL HEAT SOURCES IN MULTI LAYER INSULATED GATE BIPOLAR TRANSISTORS (IGBT)

Kelvin Chen, kelvinchen@poli.ufrj.br
Carolina Palma Naveira Cotta, carolina@mecanica.coppe.ufrj.br
Christopher Peter Tostado, tostado@gmail.com
Philippe Rollemberg d'Egmont, philippe@poli.ufrj.br
Fernando Pereira Duda, duda@mecanica.coppe.ufrj.br
Antonio Guilherme Barbosa da Cruz, aguicruz@mecanica.coppe.ufrj.br
Marcio Sampaio, marciosampaio@ufrj.br

Laboratory of Nano- and Microfluidics and Microsystems, LabMEMS, Mechanical Engineering Dept. (PEM) & Nanoengineering Dept. (PENT) – POLI& COPPE, UFRJ, Federal University of Rio de Janeiro, Rio de Janeiro, RJ, Brazil

Abstract. *The present work is aimed to demonstrate the solution of an inverse heat conduction problem dealing with the estimation of an internal heat source in a multi layer heterogeneous media, based on temperature measurements at the external surface. For the direct problem, a one-dimensional model based on the thermal resistance analogy was used. The inverse problem is solved with a Bayesian approach that is basically concerned with the analysis of the posterior probability density, which is the conditional probability of the parameters given the measurements. Simulated temperature measurements are used in the inverse analysis in order to show the capabilities of the proposed approach, and then a real experimental data is used to demonstrate the feasibility of the proposed methodology. The experimental results are provided via non-intrusive infrared thermography.*

Keywords*: inverse problem, IGBT, infra red thermography*

1. INTRODUCTION

The thermal management of electronic devices is very important since high working temperatures can be very prejudicial to the service life of electronics, especially for switching devices such as insulated gate bipolar transistor (IGBT), which basically is a power semiconductor device primarily used as an electronic switch which combine high current density with fast switching (Chang *et al.*, 2016) and are fundamental elements of power conversion and are used extensively, *e.g.*, variable frequency drives, electric cars and trains. The current flow in these devices induces fast temperature increase inside the module by the Joule effect and due to this fact, the temperature has to be controlled not to exceed a maximum pre-established value. Near this temperature, some undesirable effects like the change of electrical properties, the increase of leakage current, change of the threshold voltage and commutation time can be mentioned (Wu *et al.*1996; Sheng *et al.*, 2000). Furthermore, it is known that the high internal temperatures are responsible of multiples operational failures and also reduces drastically the reliability and the equipment life making the thermal management extremely important to the correct operation (Luo, 2002). Thus, the inverse problem can be a useful tool to the thermal management, estimating the heat-source value inside the module, helping to establish the operating range of work of the device.

An infrared camera was used in an experiment to measure temperatures at the module surface since infrared thermography is a non-intrusive technic with high definition and low uncertainty, which has already been used to study the thermal management of electronic devices (Chang *et al.*, 2016; Mital, 2006). These temperature measurements will serve as input data to the inverse problem. Also, numerical simulations and a one-dimensional model were performed to help the inverse problem analysis. The simulations were performed in the software COMSOL Multiphysics, using a 3D geometry to represent the real IGBT module. However, these numerical simulations run at high computational cost and are impracticable to use it as the direct problem in the estimation process, which evaluates several times the direct problem. Therefore, a one-dimensional model approach was used to overcome this problem, using the analogy of thermal resistance, commonly used in thermal management of electronics (Yun *et al*., 2001; Skibinski and Sethares, 1990). Using the information of temperature of the 3D simulation, a 1D model with thermal analogy could properly represent the numerical simulation with the advantage of being much simpler and lighter computationally.

Once the 1D model is defined as the direct problem, the inverse analysis can be used to estimate unknown parameters using the information of the temperature measurements (Hsu and Chu, 2004; Janicki and Napieralski, 2004). The method of Markov Chain Monte Carlo was adopted to estimate the diode heat-source using the temperature acquired by thermal images from the infrared camera.

2. EXPERIMENT

The experiment consists of acquiring temperature measures of the open IGBT module that was disconnected from the plastic case (Fig. 1.a). Each module contains two sub-models and each sub-model contains one diode and one IGBT chip. The circuit diagram is shown in Fig. 1.b. The IGBT module was fixed on a support where an infrared camera (FLIR A645Sc25°) is placed on top to take thermal images from the IGBT surface (Fig. 2). One power supply (item 7 from Fig. 2) was regulated to stabilize the voltage between the gate and emitter and another power supply (item 8 from Fig. 2) provided energy to the collector and the emitter. With this setup, three experimental configurations (cases 1-3) were tested to determine the temperature profile on the open IGBT module surface, which was painted by graphite paint with known emissivity. All the configurations are detailed in Tab. 1. The experiments were repeated at last two or three times with the mean value and the experimental error presented in Tab. 1.

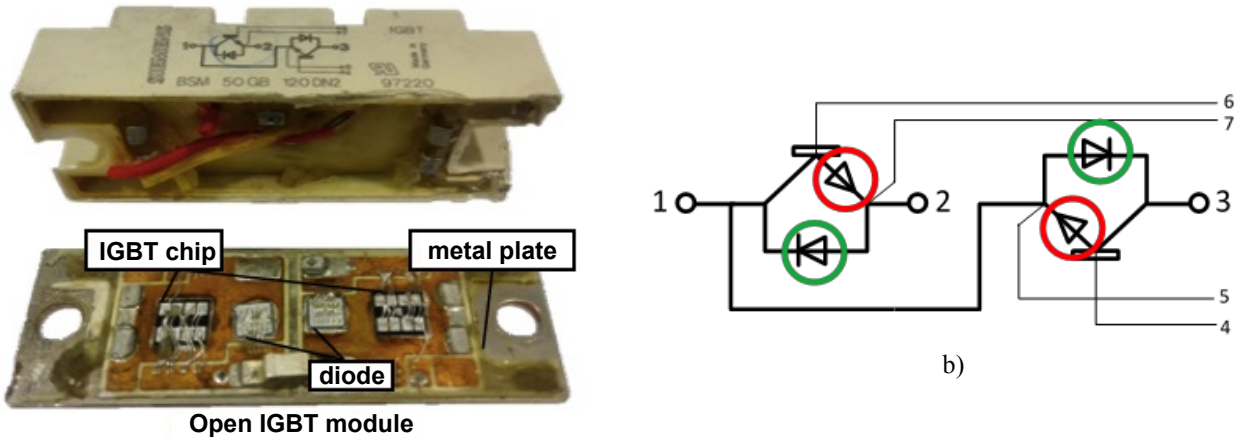

Figure 1. IGBT module (Double module Siemens BSM 50GB 120DN2): a) open and disconnected from the plastic case; b) circuit diagram, with diodes in green and IGBTs in red.

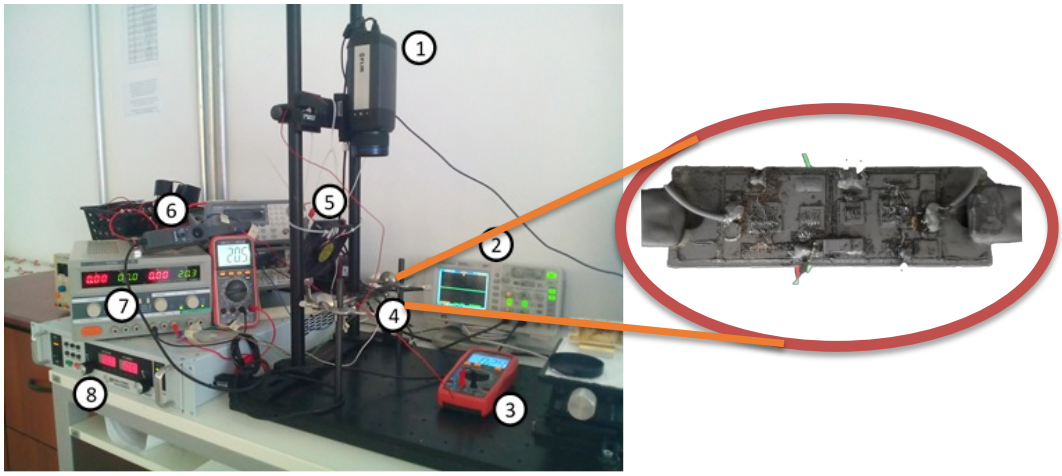

Figure 2. Experimental setup. 1- Infrared camera; 2- Oscilloscope; 3- Multimeter; 4- Siemens IGBT Module; 5- Fan; 6- Current probe; 7- High current/voltage power supply.

Table 1. Different experimental configurations with its parameters.

Case	Supplied components	Current (A)	Voltage, V_{CE} (V)	Power (W)
1	Left diode	6.15 ± 0.12	1.0	6.15 ± 0.12
2	Left IGBT	4.91 ± 0.10	1.25	6.14 ± 0.12
3	Right diode	6.16 ± 0.12	1.0	6.16 ± 0.12

The results of the three configurations showed in Tab. 1 are presented in Fig. 3. Also, it is presented some thermal images for different times for the experiment of case 1. As we can see, the ΔT for the three cases 1, 2 and 3 are almost equal with ΔT of 44.25°C, 44.93°C, e 44.92°C, respectively. These temperature values will be used as comparison with the numerical simulation as well as information for the estimation process in the inverse analysis. For the thermal images, the location of maximum temperature is indicated by a red triangle and the location of minimum temperature by

a blue triangle. The black rectangle delimits the area where the temperature measurements are taken. As it is shown in Fig. 3, for short times, that is, in the beginning of the experiment, the area which the left diode is positioned coincides with the area which has the highest temperature. It occurs due to the fact that in this experiment, the supplied component is the left diode which contains a heat-source due to the current and voltage, dissipating power (Fig 3.a). As time proceeds, the temperature in the module tends to be more uniform since the heat is spreading to the rest of the components, but the highest temperature measured still remains in the left diode area (Fig. 3.b). For higher times, when the steady state is reached, the temperature does not increase anymore and the temperature is more uniform than shorter times, but the highest temperature still occur in the left diode (red triangle), which is expected since the heat-source is located in the left diode (Fig. 3.c).

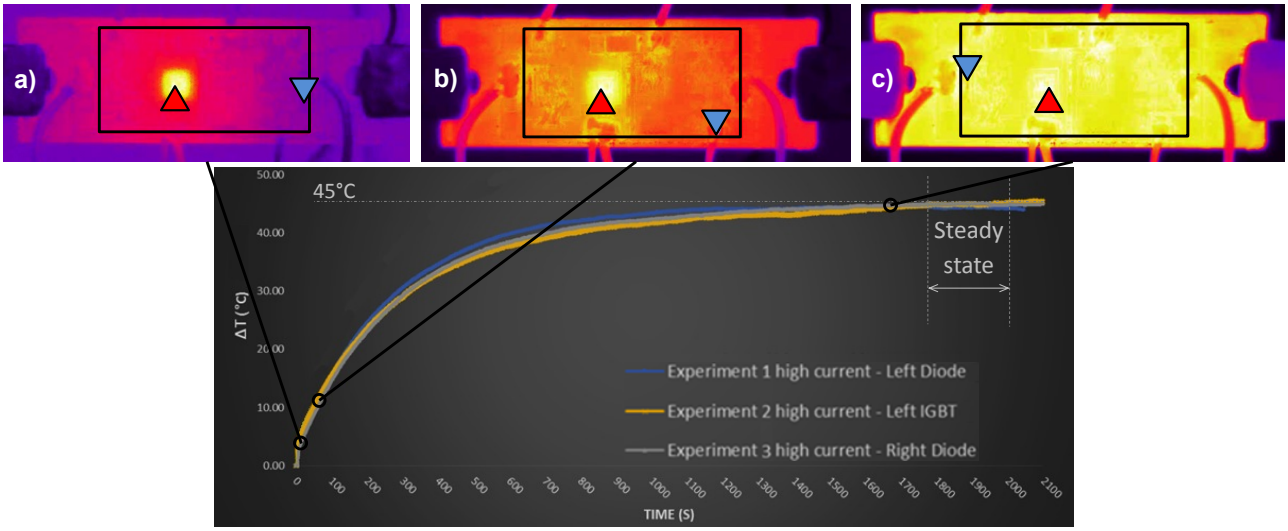

Figure 3. Maximum IGBT surface ΔT for the cases 1, 2 and 3.

3. NUMERICAL SIMULATION

Numerical simulations of the 3D geometry representing the IGBT module used in the experiment described previously were performed using the software COMSOL Multiphysics (Fig. 4). It was considered that the module is composed by five different materials, each one forming a layer as we can see in Fig. 4. The properties used in the simulation are described in Tab. 2, where h_1 is the convection heat transfer coefficient of the top surface (layer 1) and h_5 of the bottom surface (layer 5). Their values were determined by convection heat transfer correlations (Ozisik, 1985). The parameter h_r is the radiation heat transfer coefficient, calculated with the emissivity of the graphite paint (ε=0.97) for the top surface and for the bottom surface an emissivity value of ε=0.05, referred to a polished metal (Minkina and Dudzik, 2009). The parameters σ and T_∞ denote, respectively, the Stefan-Boltzmann constant (σ=5.67× 10^{-8} W/(m²K⁴)) and the room temperature. The parameter *Pot* is the power and *g* is the heat-source, calculated by the power divided by the volume of the layer where it is imposed. The properties used in this simulation were chosen to recreate the case 1 in Tab. 1.

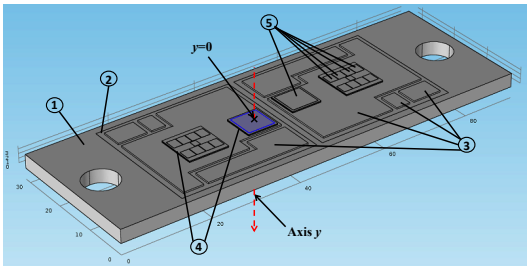

Figure 4. Geometry used in 3D simulation with heat source in the left diode.

Table 2. Properties used in simulation.

Layer	Material	Thickness [mm]	Density [kg/m³]	Thermal cond. [W/(mK)]	Specific heat [J/(kgK)]
1	Aluminum	0.07	2700	237	900
2	Silicon	0.314	2330	148	700
3	Copper	0.286	8920	400	380
4	Al_2O_3	0.668	3960	20	753
5	AlSiC-9	3	3000	180	434
h_1=10 W/(m²K)			h_5=12 W/(m²K)		
$h_r = 4\varepsilon\sigma T_\infty^3$			$T_{initial}=T_\infty$=25 °C		
Vol=6 mm × 6 mm × 0.7 mm = 2.52 mm³ = 2.52 × 10^{-9} m³					
Pot=6.15 W			*g*=*Pot*/*Vol*=2.44× 10^{-9} W/m³		

Before running the simulations, a mesh convergence analysis was carried out to determine the influence of the mesh size on the simulation results. Two analyses were performed: spatial, where three meshes were used, named N1, N2 and

N3; and temporal, where another three meshes were used, M1, M2 and M3. The meshes are detailed in Tab. 3 and Tab. 4.

Table 3. Different spatial meshes.

Mesh	Max. Element Size	Num. of elements
N1	0.5 mm	164900
N2	0.3 mm	680244
N3	0.2 mm	1393064

Table 4. Different temporal meshes.

Mesh	Step time	Num. of elements
M1	100 s	20
M2	50 s	40
M3	25 s	80

The results for both analyses are presented in Tab. 5 and Fig. 6, for the spatial mesh and Tab. 6 and Fig. 7, for the temporal mesh. As we can see in Tab. 5, the relative errors between the meshes are very low for different positions, which mean that the size of the mesh has no significant influence in the temperature results. The same behavior is noticed in Tab. 6, where the relative errors between meshes are very low again. So, the mesh N1 and M1 was chosen to run the simulations.

Table 5. Relative errors between the spatial discrete meshes.

y (mm)	Rel. error N1 and N2 (%)	Rel. error N2 and N3 (%)
0	0.0076738	0.00180411
0.07	0.00767585	0.00180421
0.384	0.00762821	0.00179341
0.67	0.00755325	0.00177572
1.338	0.00164767	0.000384905
4.338	0.00093093	0.000212521

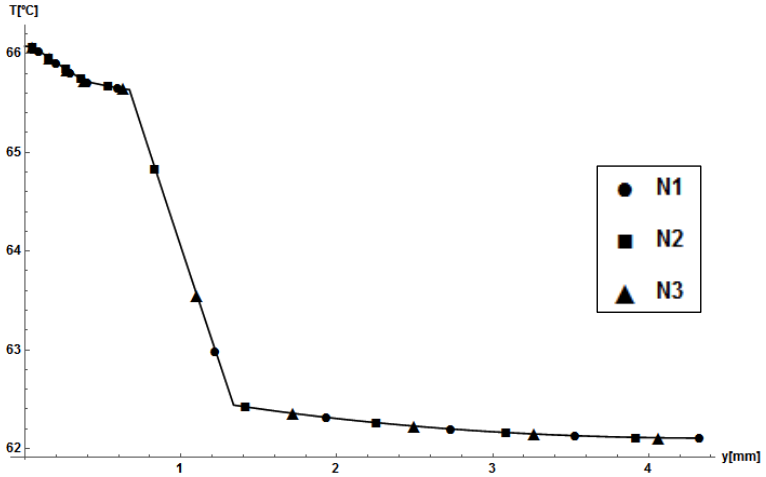

Figure 5. Comparison of special discrete meshes.

Table 6. Relative errors between the time discrete meshes.

Time (s)	Rel. error M1 and M2 (%)	Rel. error M2 and M3 (%)
500	0.145328	2.994×10^{-10}
1000	0.000024707	9.64×10^{-13}
1500	0.00671847	1.548×10^{-10}

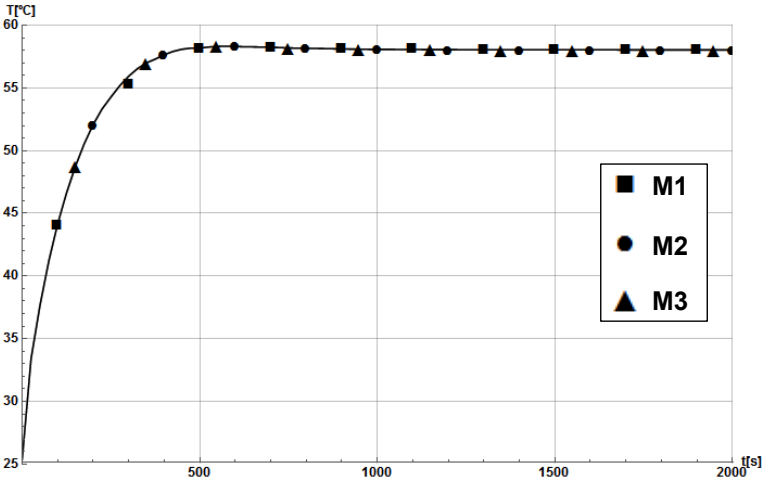

Figure 6. Comparison of time discrete meshes

With the meshes defined, simulation was run for the case 1 showed in Tab. 1. The comparison of simulation and experiment are shown in Fig. 7. We can notice that for the initial time, there is a significant difference between the temperatures. But as long as the experiment time runs, both results show a better agreement at steady state, with temperature differences of only 1.96 ºC, about 2.75% of relative error.

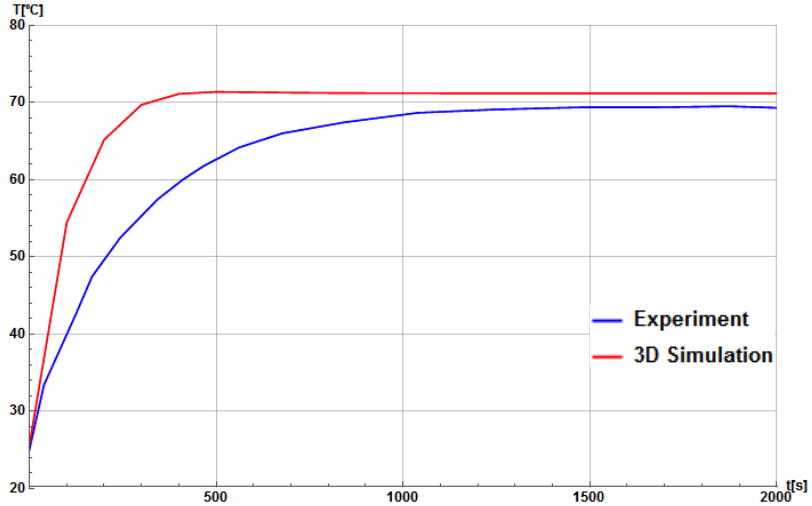

Figure 7. Comparison between experiment and 3D simulation and thermal images for different times of experiment.

4. ONE-DIMENSIONAL MODEL

A steady state one-dimensional model was built to describe the temperature profile of the IGBT module to make easier the process of the parameter estimation, since a three-dimensional model is too expensive computationally and the estimation process require a high number of evaluations of the direct problem. It can be done by applying the thermal resistance analogy (Ozisik, 1985). The method used is similar to the thermal network (Luo, 2002). The thermal resistances can be calculated with a curve fitting using the information of temperature from an experiment (Skibinski and Sethares, 1990) or from a numerical simulation (Yun *et al.*, 2001). The 1D model scheme is presented in Fig. 8, where M_i and L_i represent the material and the thickness of the layer i, respectively. $\bar{T}_i$ and y_i represent the temperature at the interfaces and the interface position, respectively. The parameters used in the 1D model are the same specified in Tab. 2. So the thermal resistances can be calculated by (Ozisik, 1985):

$$R_i^* = \frac{\bar{T}_{i-1} - \bar{T}_i}{Q}, \text{ where } \begin{array}{l} i: \text{ Layer Number} \\ \bar{T}_i: \text{Temperature at interface } i \end{array} \quad (1)$$

The thermal resistances values are presented in Tab. 7. They were calculated using the information of temperature of the 3D simulation with the properties of Tab. 2, *i.e.*, with a heat source of value g. There is no thermal resistance at the first layer since it was considered a heat source, making the temperature profile at this layer not linear but parabolic so it cannot be used the thermal resistance analogy.

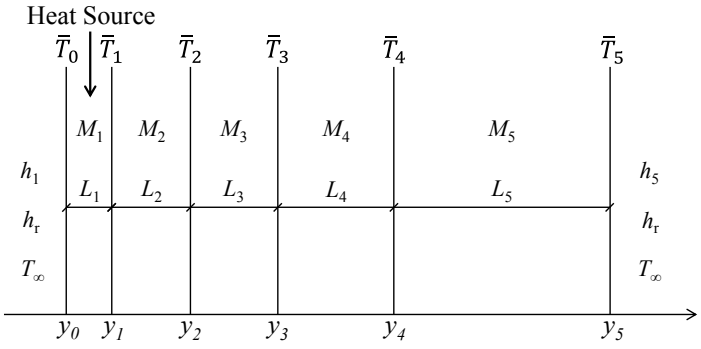

Figure 8. 1D heterogeneous media model with heat source.

Table 7. Values of the thermal resistances.

Layer	Value (K/W)
R_2	0.000462146
R_3	0.000121871
R_4	0.0044787
R_5	0.000467793

With the thermal resistances calculated with an imposed heat-source g in the first layer, the 1D temperature profile was compared to the 3D simulation (Fig. 9). It was shown that with these values of resistance, the 1D model could represent well the 3D simulation. In order to check the reliability of the method, another three values of heat-source were imposed in the simulation and compared with the 1D model with the thermal resistances calculated previously (Tab. 7). As can be seen, the relative error is very low for all the cases, showing that the 1D model could be a good approximation of the 3D model, helping the reduction of computational time in the estimation process describe later.

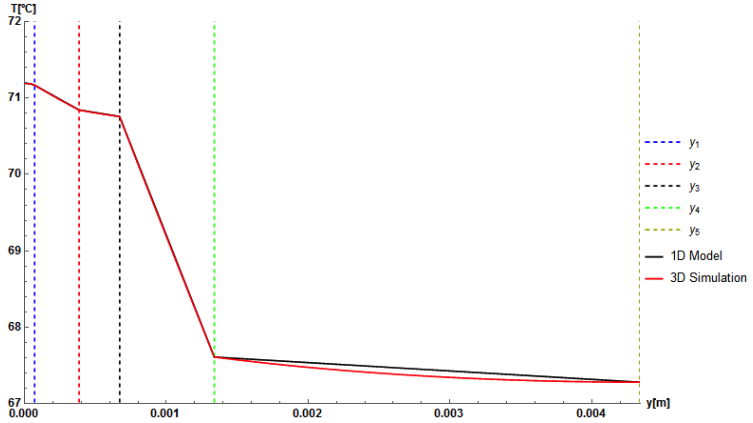

Figure 9. Comparison of 1D model with 3D simulation.

Table 8. Relative error (%) from the comparison of the results with different heat source values.

	Heat Source		
y (mm)	$0.5g$	$2g$	$3g$
0.07	0.202365	1.26078	3.27651
0.384	0.202372	1.26093	3.27706
0.67	0.202459	1.26296	3.28436
1.338	0.202479	1.26347	3.28622
4.338	0.203049	1.28165	3.35371

5. INVERSE PROBLEM

The next step is the inverse analysis and parameter estimation process. In this work, the method of Markov Chain Monte Carlo was adopted. It consists in an iterative process where each iteration depends only on the previous iteration that, in general, has a well-defined limit behavior when a sufficient number of iterations is achieved. Then, at the end of the iteration process, the parameter estimated is determined from the statistical evaluation of the results.

Inverse problems are classified as ill-posed while the direct problems are well-posed. (Beck and Arnold, 1977; Alifanov, 1994; Ozisik and Orlande, 2000). Estimation problems with Bayesian approach has two components: the likelihood function of **P**, $p(\mathbf{Y}|\mathbf{P})$, which provides information about the chance of each value of **P** have led to that observed value for **Y**, and the distribution $p(\mathbf{P})$, called *prior* density, which contains the probability distribution of **P** before the observation of the value **Y**. It is reasonable that the inference process is based on the probability distribution of **P** after watching the value of **Y**. This distribution, $p(\mathbf{P}|\mathbf{Y})$, is called a *posteriori* distribution, obtained by the Bayes theorem in Eq. (2).

$$p(\mathbf{P}|\mathbf{Y}) = \frac{p(\mathbf{Y}|\mathbf{P})p(\mathbf{P})}{p(\mathbf{Y})} = \frac{1}{const}\,p(\mathbf{Y}|\mathbf{P})p(\mathbf{P}) \tag{2}$$

where: $\mathbf{P} = \{P_j\}, j = 1,...,N_{par}$ Unknown parameters vector; N_{par} : Number of parameters

$\mathbf{Y} = \{Y_s\}, s = 1,...,N_{meas}$ Experimental measures vector; N_{meas} : Number of measures

Once obtained the *posteriori* distribution, we can summarize the information contained by calculating statistical measurements like the mean value, mode, median, variation and standard deviation, precision and mode curvature. Thus, the *posteriori* probability density function could be described by being proportional to the product of the likelihood and the *priori* distribution:

$$p(\mathbf{P}|\mathbf{Y}) \propto p(\mathbf{Y}|\mathbf{P})p(\mathbf{P}) \tag{3}$$

Assuming that the temperature data are independent and identical distributed, the likelihood can be written as:

$$p(\mathbf{Y}|\mathbf{P}) = \frac{1}{\left(2\pi\sigma_{\mathbf{Y}}^2\right)^{-1/2}}\,\mathrm{Exp}\left[\frac{\left(\mathbf{Y}-T(\mathbf{P})\right)^T\left(\mathbf{Y}-T(\mathbf{P})\right)}{2\sigma_{\mathbf{Y}}^2}\right] \tag{4}$$

where $T(\mathbf{P})$ is the temperature calculated as a function of the parameters to be estimated and **Y** are the measured temperatures. The Metropolis-Hastings algorithm was used in the Markov Chain Monte Carlo method (Metropolis *et.al.*, 1953; Hastings, 1970; Gamerman and Lopes, 2006). The algorithm uses a probability density function $\pi(\mathbf{P}^*|\mathbf{P})$. Supposing that the chain is in a state **P**, a new candidate value $\mathbf{P}^*$ is generated from the auxiliary distribution $\pi(\mathbf{P}^*|\mathbf{P})$ and is accepted with the probability described by the Eq. (5), where α is called Hastings ratio.

$$\alpha(\mathbf{P}^*|P) = \min\left[1, \frac{p(\mathbf{P}^*|\mathbf{Y})\pi(\mathbf{P}^*|\mathbf{P})}{p(\mathbf{P}|\mathbf{Y})\pi(\mathbf{P}|\mathbf{P}^*)}\right] \tag{5}$$

where $p(\mathbf{P}|\mathbf{Y})$ is the *posteriori* distribution of interest. To begin the estimation process, it is necessary to define a range with a minimum and a maximum value of search as well as an initial guess for the iterative process. It is necessary to define the number of states to the iteration and also the number of states that will be discarded, which is assumed that the iteration did not reach the equilibrium at these initial states, called heat states.

5.1 Simulated temperature measurements

Firstly, an analysis using a simulated temperature measurement was done in order to test the reliability of the one-dimensional model in the estimation process. In this step, one simulated measured temperature, located at the surface of the left diode (colored in blue in Fig. 4), was adopted as the input data, since it is used the one-dimensional model and only one temperature is defined for each interface layer. The simulated measured temperature was calculated by Eq. (6). The properties used in this analysis are described in Tab. 9. Figure 10 shows the Markov chains resulted from the estimation process using the properties in Tab. 9. Table 10 shows the results after the statistical evaluation and Fig. 11 shows the frequency distribution of the estimated values in the MCMC method. A different value of heat-source was chosen to not run this test case with the value g, which was used to calculate the one-dimensional model. So the value of $2.5g$ was chosen as the exact value of heat-source for this test case.

$$Y = T_{exact} + \varepsilon, \qquad \varepsilon: \text{ Random number with normal distribution } [0,\sigma] \tag{6}$$

Table 9. Properties of MCMC method for the heat source estimation.

Exact value	$2.5g$
Measures	1
Standard deviation (σ)	5ºC
Priori distribution	Uniform
{Minimum value, Maximum value}	{0, $3g$}
Initial guess	$0.01g$
Number of states	5000
Heating states considered	1250

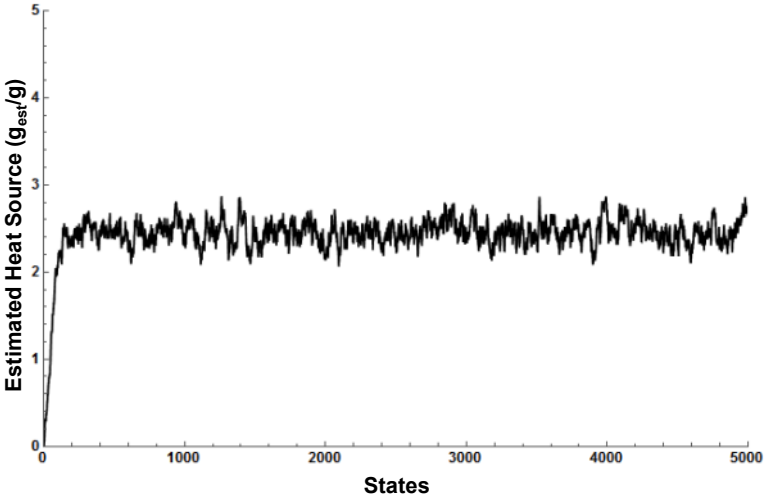

Figure 10. Markov chains for the simulated measures.

Table 10. Results of the MCMC method.

Accepted states	4313
Estimated mean value	$2.4483g$
Confidence interval (99%)	{$2.13324g$, $2.76336g$}

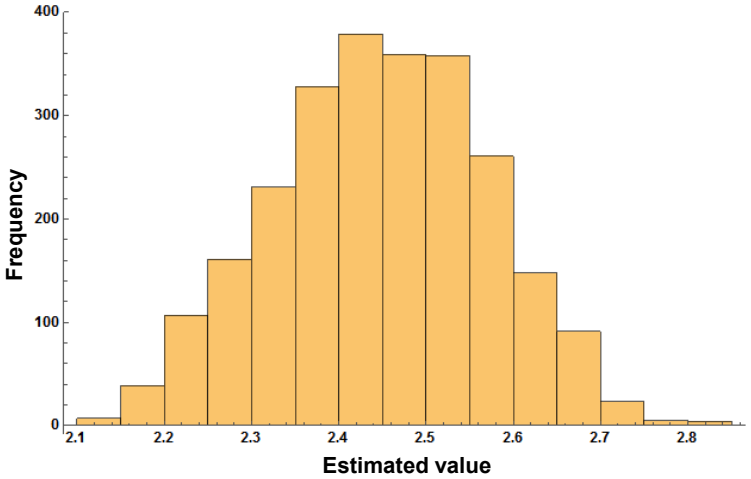

Figure 11. Histogram distribution of the estimated values.

As can be seen in Fig. 10, which shows the ratio between the estimated heat-source and g, the chains were oscillating around values closer to 2.5, which is the expected value. It is confirmed in Tab. 10, which shows the mean value of the estimation and the confidence interval with 99%. As we can see, the estimated mean value is very close to the expected ($2.5g$) and the exact value is in the confidence interval. It means that the MCMC method with the one-dimensional model as the direct problem could estimate the heat-source with the parameters listed in Tab. 9.

5.2 Real temperature measurement

After the test case, real measured temperature was used to run the MCMC method, using the one-dimensional model as the direct problem, which will make the inverse problem viable due to the reduced computational cost. One value of temperature measurement at the left diode surface, acquired by the experiment referred to the case 1 in Tab. 1, at the steady state, was taken by the infrared camera and was adopted as input data. The properties of the iteration method are described in Tab. 11. Figure 12 shows the Markov chains resulted from the estimation process using the properties in Tab.11. Table 12 shows the results after the statistical evaluation and Fig. 13 shows the frequency distribution of the estimated values in the MCMC method.

Table 11. Properties of MCMC method for the heat source estimation.

Calculated heat source	
Measures	1
Standard deviation	5ºC
Priori distribution	Uniform
{Minimum value, Maximum value}	{0,3*g*}
Initial guess	0.01*g*
Number of states	5000
Heating states considered	1250

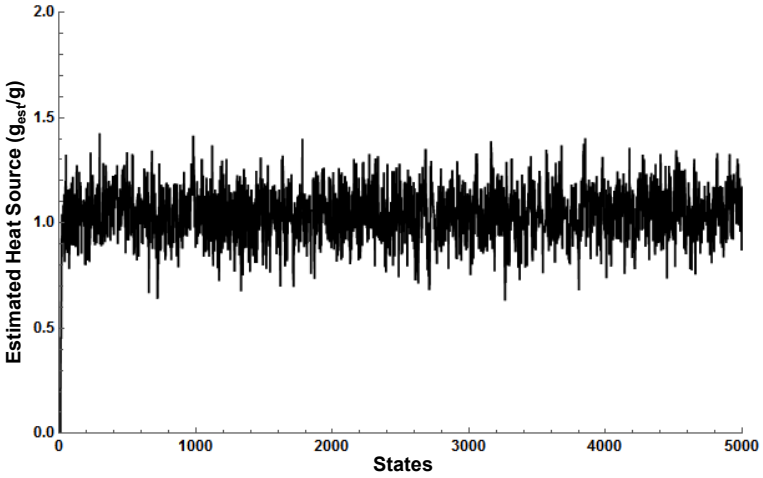

Figure 12. Markov chains for estimation of heat source of the experiment.

Table 12. Results of the MCMC method.

Accepted states	2735
Estimated mean value	1.04744*g*
Confidence interval (99%)	{0.73971*g* , 1.35517*g*}

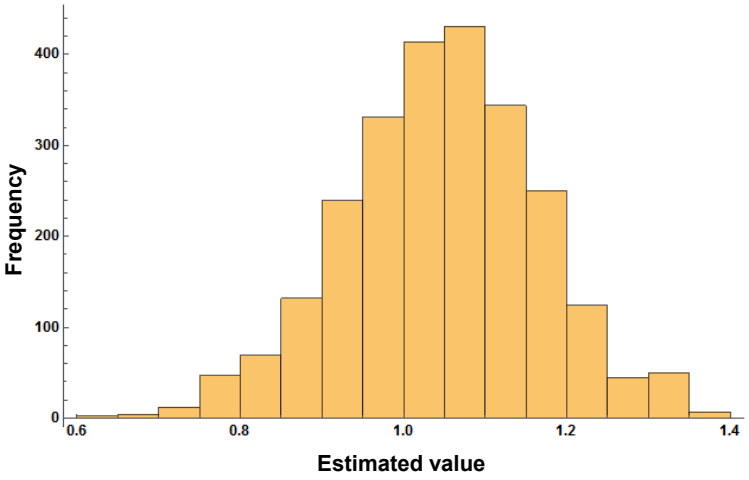

Figure 13. Histogram distribution of the estimated values.

As can be seen in Fig. 12, which shows the ratio between the estimated heat-source and *g*, the chains were oscillating around values closer to 1, which is the expected value. This is confirmed in Tab. 12, which shows the mean value of the estimation and the confidence interval with 99%. As we can see, the mean value estimated is very close to the expected (*g*) and the exact value is in the confidence interval. It means that the MCMC method with the one-dimensional model as the direct problem could estimate the heat-source with the parameters listed in Tab. 11 with real temperature measures taken with the infrared camera.

6. ACKNOWLEDGEMENTS

The authors acknowledge the financial support of the sponsoring agencies CNPq, FAPERJ and GE- General Electric Company.

7. REFERENCES

Alifanov, O. M., 1994. Inverse Heat Transfer Problems. Springer-Verlag, New York.

Beck, J. V., Arnold, K. J., 1977. Parameter estimation in engineering and science. John Wyley and Sons, New York.

Chang, T. C., Fuh, Y. K., Lu, H. Y., Tu, S. X., 2016. "Thermal management and performance evaluation of a dual bi-directional, soft-switched igbt-based inverter for the 1st autonomous microgrid power system in taiwan under various operating conditions". Heat and Mass Transfer, Vol. 52, No. 6, pp. 1231–1241.

Gamerman, D., Lopes, H. F., 2006. Markov Chain Monte Carlo Stochastic Simulation for Bayesian Inference. Second Edition. CRC Press, London.

Hastings, W. K., 1970. "Monte Carlo Sampling Methods Using Markov Chains and Their Applications". Biometrika, Vol. 57, No. 1, pp. 97-109.

Hsu, P. T., Chu, Y. H., 2004. "An inverse non-Fourier heat conduction problem approach for estimating the boundary condition in electronic device". Applied Mathematical Modelling, Vol. 28, pp. 639-652.

Janicki, M., Napieralski, A., 2004. "Inverse heat conduction problems in electronics with special consideration of analytical analysis methods". In Proceedings of the CAS 2004 Semiconductor Conference, Vol. 2, pp. 455-458.

Liao, L. L, Hung, T. Y., Liu, C. K., Li, W., Dai, M. J., Chiang, K. N., 2014. "Electro-thermal finite element analysis and verification of power module with aluminum wire". Microelectronic Engineering, Vol. 120, pp. 114-120.

Luo, Z., 2002. A thermal model for igbt modules and its implementation in a real time simulator. Ph.D. thesis, University of Pittsburgh, Pittsburgh, PA, USA.

Metropolis, N., Rosenbluth, A. W., Rosenbluth, M. N., Teller, A. H., 1953. "Equation of state calculations by fast computing machines". The Journal of Chemical Physics, Vol. 21, No. 6, pp. 1087-1092.

Minkina, W., S. Dudzik, S., 2009. Infrared Thermography: Errors and Uncertainties. Wiley, New York.

Mital, M., 2006. Integrated thermal management strategies for embedded power electronic modules. Ph.D. thesis, Virginia Polytechnic Institute and State University, Blacksburg, VA, USA.

Ozisik, M.N., 1985. Heat Transfer – A Basic Approach. McGraw Hill, New York.

Ozisik, M. N., Orlande, H. R. B., 2000. Inverse Heat transfer: Fundamentals and Applications. Taylor & Francis, New York.

Sheng, K.; Finney, S. J.; Williams, B. W., 2000. "Thermal stability of igbt highfrequency operation". Industrial Electronics, IEEE Transactions on Industrial Electronics, Vol. 47, No. 1, pp. 9-16.

Skibinski, G. L., Sethares, W. A., 1991. "Thermal Parameter Estimation Using Recursive Indentification". IEEE Transactions on Power Electronics, Vol. 6, No. 2, pp. 228-239.

Wu, W.; Gao, G.; Dong, L.; Wang, Z.; Held, M.; Jacob, P.; Scacco, P., 1996. "Thermal reliability of power insulated gate bipolar transistor (IGBT) modules". In proceedings of the Semiconductor Thermal Measurement and Management Symposium, pp. 136–141

Yun, C. S., Malberti, P., Ciappa, M., Fichtner, W., 2001. "Thermal Component Model for Electrothermal Analysis of IGBT Module Systems". IEEE Transactions on Advanced Packaging, Vol. 24, No. 3, pp. 401-406.

8. RESPONSIBILITY NOTICE

The authors are the only responsible for the printed material included in this paper.